Astron. Astrophys. 356, 559–569 (2000)

ASTRONOMY AND ASTROPHYSICS

Closure in flux-limited neutrino diffusion and two-moment transport

J.M. Smit[1,2], **L.J. van den Horn**[2,3], **and S.A. Bludman**[2,4,5]

[1] Space Research Organization Netherlands, Sorbonnelaan 2, 3584 CA Utrecht, The Netherlands
[2] Center for High Energy Astrophysics, University of Amsterdam, Kruislaan 403, 1098 SJ Amsterdam, The Netherlands
[3] Institute for Theoretical Physics, University of Amsterdam, Valckenierstraat 65, 1018 XE Amsterdam, The Netherlands
[4] University of Pennsylvania, Department of Physics and Astronomy, 209 South 33rd Street, Philadelphia, PA 19104-6396, USA
[5] DESY, Notkestrasse 85, 22603 Hamburg DESY, Hamburg, Germany

Received 21 September 1999 / Accepted 28 January 2000

Abstract. Two-dimensional maximum entropy closure and various standard one-dimensional closures in flux-limited neutrino diffusion and two-moment transport are compared against direct numerical solutions of the neutrino Boltzmann equation. The approximate transport based on particular closures of the moment equations is rated by testing so-called weak equivalence of the first three moments of the neutrino radiation field. Additionally we consider strong equivalence of the maximum entropy angular model distribution. Our calculations are performed on two different matter backgrounds and involve several neutrino energies. As an alternative multiple energy test we look at the behavior of spectral and energy-averaged Eddington factors. Among the closures considered, two-dimensional maximum entropy closure is found to overall approximate most closely the full transport solutions.

Key words: radiative transfer – methods: numerical – stars: atmospheres – stars: neutron – stars: supernovae: general

1. Introduction

In radiative systems radiation is invariably transported through the medium. The transport equation, therefore, is the basic equation underlying the radiative hydrodynamics. In practice one commonly circumvents this fundamental equation by resorting to some simplifying procedure to approximate the transport problem. Although computationally intensive, the Boltzmann equation can nowadays be solved numerically in one spatial dimension. Nevertheless, semi-analytic approximation schemes are needed in higher dimensional problems, and are often more illuminating than exact treatments, even in one dimension. The physical foundation for a particular choice of approximation, however, is not always in evidence, and the ensuing physical description of the system may be rather qualitative.

Currently fashionable approximations are flux-limiting prescriptions and closure relations for the moment equations, a number of which we shall examine below. Although flux-limiting and the moment method are essentially different approaches to deal with anisotropic radiation fields, the two are connected through a generic relationship between flux limiter and Eddington factor (*cf* Sect. 2). In this paper we focus on two-moment transport, and check a number of closure relations against direct numerical solutions of the Boltzmann equation. We will do so within the scope of fermionic (neutrino) radiation. Previous investigations in this field (Janka 1991, 1992; Janka et al. 1992; Cernohorsky & Bludman 1994) have revealed a number of shortcomings of standard closures and have proposed possible improvements. One such improved treatment is provided by two-dimensional maximum entropy closure. While the numerical overhead of any two-dimensional closure would easily appear at odds with the attempt for computational economy, it has proven possible, in the case of Fermi-Dirac statistics, to formulate an efficient closure algorithm (Cernohorsky & Bludman 1994).

There is no such thing as the "correct" closure. At most one may strive for a closure which is able to describe the radiation field "as well as possible" in a given transport problem. The quick way is to adopt an *ad hoc* relation, for example one that smoothly interpolates between the diffusive and free-streaming fluxes, such as Wilson's closure (Sect. 3.2.1). Or one may look for such a relation based on geometrical or other considerations. Alternatively, the closure can be derived from a given or assumed angular dependence of the radiative distribution function. In some cases the functional dependence obtained from direct transport calculations may serve to model the closure, as is the case for Janka's Monte Carlo closure (Sect. 3.2.3).

An appealing approach is to derive the angular dependence from a basic principle. In this spirit the maximum entropy closure (Minerbo 1978) and the Levermore-Pomraning closure (Levermore & Pomraning 1981), discussed in Sects. 3.1 and 3.2.2, have been obtained. These were derived originally for the case of photon radiation, and have subsequently been applied to neutrino transport as well. For photon radiation more closures can be found in the literature (Levermore 1984).

The Wilson and Levermore-Pomraning closures have become standard in neutrino transport calculations. Implementation is commonly effected through use of the corresponding

Send offprint requests to: J.M. Smit
Correspondence to: m.smit@sron.nl

flux limiters in a flux-limited diffusion (FLD) scheme. In our calculations for this paper we employed a two-moment transport (TMT) scheme incorporating maximum entropy closure (MEC) besides various other closures. The philosophy behind MEC is that it allows for the least biased distribution of the radiation quanta based on the available information, *viz.* particle statistics, energy or occupation density, and flux. The dependence on energy density in addition to the flux calls for an inherently two-dimensional closure which may contain more traditional one-dimensional closures as limiting cases.

If TMT with a given closure is to be successful, the TMT solution should approximate, as closely as possible, the first three angular moments of the exact distribution, for each point in space and for every energy. Beyond this "weak equivalence" of the angular moments, one may also consider "strong equivalence" of a given model distribution, *i.e.*, judging whether or not the exact distribution is well represented by the model distribution (Cernohorsky & Bludman 1994).

In Sect. 2 we briefly outline the procedures of flux-limited diffusion and two-moment transport. Though offering different perspectives, an intimate relation exists between their central concepts of flux limiter and closure. Various closures are reviewed in Sect. 3. In Sect. 4 the validity of approximate transport is evaluated in terms of the concepts of weak and strong equivalence of the angular distribution and its moments. For this purpose we consider two different material backgrounds and a number of neutrino energies. We also examine the behavior of spectral and of energy averaged Eddington factors. Among the closures considered, two-dimensional MEC appears to give the best overall approximation to the full Boltzmann transport calculations, while the Wilson and Levermore-Pomraning closures are poorest. Our conclusions are summarized in Sect. 5.

2. Flux-limiting and two-moment transport

The essential simplification in both flux-limited diffusion and the two-moment approach consists in discarding the detailed angular information contained in the radiation field. Instead one considers angular averages ('moments') of the distribution function. The first three are the radiative energy density E, energy flux $\mathbf{F}$, and pressure tensor P, respectively. The basic assumption is that these quantities suffice as a physical description of the radiation field. The moments must satisfy the energy and momentum equations

$$\partial_t E + \nabla \cdot \mathbf{F} = \kappa_a (B - E) \quad , \tag{1}$$

$$\partial_t \mathbf{F} + \nabla \cdot \mathsf{P} = -\kappa \mathbf{F} \quad , \tag{2}$$

which are obtained by angular integrations of the radiative transport equation. Here κ_a and κ are the absorptive and total transport opacities, respectively, and $B = B(T)$ is the 'blackbody' thermal energy density. In these equations, the velocity of light has been put equal to one. Eqs. (1) and (2) may be read as monochromatic (spectral) as well as energy integrated equations.

The classical closure problem is that, because there are more physical variables than equations, an additional relation must be supplied to close the set. One important closure is the diffusion approximation (Fick's Law)

$$\mathbf{F} = -\frac{c}{3\kappa}\nabla E \equiv \frac{1}{3} c E \mathbf{R} \quad , \tag{3}$$

where $R \equiv |\nabla E|/\kappa E$, the ratio of mean free path to energy scale height, is the Knudsen number. Where small opacities or steep gradients make $R \gg 1$, Fick's Law would allow an acausal flux, $F > cE$. The flux-limiting remedy is to modify (3) to

$$\mathbf{F} = cE\lambda(R)\mathbf{R} \quad , \tag{4}$$

where the *flux limiter* $\lambda(R)$ is specifically designed to meet the causality requirement

$$\lim_{R\to\infty} R\lambda(R) = 1 \tag{5}$$

and the correct diffusion limit

$$\lim_{R\to 0} \lambda(R) = \frac{1}{3} \quad . \tag{6}$$

Flux-limited diffusion, therefore, is a minimal moment approach, taking into account only the energy Eq. (1) as an angular moment equation, with a closure at the lowest level.

In the two-moment description closure is expressed by two Eddington factors

$$\mathbf{f} \equiv \mathbf{F}/Ec \quad , \quad \mathsf{p} \equiv \mathsf{P}/E. \tag{7}$$

It is usually assumed that p does not explicitly depend on the energy density, *i.e.*, a 'one-dimensional' closure prescription, $\mathsf{p} = \mathsf{p}(\mathbf{f})$, is adopted. In principle, however, one has a 'two-dimensional' relationship

$$\mathsf{p} = \mathsf{p}(\mathbf{f}, e) \tag{8}$$

among the first three reduced moments

$$\{e,\, e\mathbf{f},\, e\mathsf{p}\} \equiv (4\pi)^{-1} \int d^2\Omega \{1,\, \mathbf{\Omega},\, \mathbf{\Omega\Omega}\} \mathcal{F}(\mathbf{\Omega}) \tag{9}$$

of the radiative distribution function $\mathcal{F}$. (Here $\mathbf{\Omega}$ is the direction of the momentum vector of the radiation quanta.) In systems with local axial symmetry (such as plane and spherical geometries), Eq. (8) reduces to a scalar relationship, $p = p(f, e)$, because there is a preferred direction. The variable Eddington factor $p(f, e)$ must satisfy

$$\lim_{f\to 0} p(f,e) = 1/3 \quad , \quad \lim_{f\to 1} p(f,e) = 1 \quad , \tag{10}$$

in order that the radiation field have the correct diffusive and free-streaming limits. The constraint (Levermore 1984)

$$f^2 \le p \le 1 \tag{11}$$

follows from f and p being normalized averages of a distribution, cf. Eq. (9). Note that the quantities (9) are spectral and space & time dependent through $\mathcal{F}$.

As Eqs. (4) and (7) show, a flux limiter λ is directly related to the Eddington flux factor f. Any variable Eddington factor

p may be used to construct a flux limiter according to (Levermore 1984)

$$\lambda(R) = p - f^2 \geq 0 \tag{12}$$

where the inequality follows from (11). Levermore (1984) presents a variety of closures with their associated flux limiters.

Two-moment transport (TMT) and flux-limited diffusion (FLD) are thus closely related. In TMT the closure is at the level of the momentum equation ('2nd moment closure'), while in FLD the momentum equation is formally ignored ('1st moment closure'). It is possible to quantify the error in the momentum balance (Cernohorsky & van den Horn 1990) and to compensate for it by introducing an 'artificial' opacity (Janka 1991) into the Knudsen parameter R, Eq. (3), which effectively reinstates the neglected momentum contributions. In this way a modified FLD scheme results which should correctly account for energy-momentum balance. Such a scheme was first presented in the context of neutrino transport by Janka (1991) and Dgani & Janka (1992) as an alternative approach to TMT with a variable Eddington factor. However, while the conceptual framework of FLD is formally preserved, the extended FLD scheme is equivalent to the set of TMT equations. Strictly then, one is no longer solving a diffusion equation, *i.e.*, a parabolic partial differential equation. The moment equations are actually a hyperbolic set.

The hyperbolicity of the moment equations has implications for any approximate solution procedure involving a closure on the variable Eddington factor. In particular, with a nonlinear closure, physically acceptable solutions meeting prescribed boundary conditions may be out of (numerical) reach. As shown by Körner & Janka (1992), the solutions contain a critical point, so that nearby solutions easily diverge away from the physical solution. Smit et al. (1997) have shown under what conditions the physical solution is stably and accurately mimicked.

A hyperbolic system admits discontinuity waves. In the free-streaming case, singularities must progagate with the speed of light. This causality requirement implies (Anile et al. 1991)

$$\left(\frac{\partial p}{\partial f}\right)_{f=1} = 2 \quad . \tag{13}$$

This constraint on the closure is supplementary to the set (10)-(11), but has not been imposed in standard closures. In the next section, we will see that (13) is met by all fermionic maximum entropy closures, but not by the Wilson and Levermore-Pomraning closures.

3. Closures

3.1. Maximum entropy closure

The use of a maximum entropy principle to find a closure dates back to Minerbo (1978), who applied the procedure to photon transport. Cernohorsky et al. (1989) first applied the principle to fermionic radiation. By maximising the spectral entropy functional

$$S[\mathcal{F}(\mu)] = -\int_{-1}^{1} d\mu [\,\mathcal{F}\ln\mathcal{F} + (1-\mathcal{F})\ln(1-\mathcal{F})\,] \quad , \tag{14}$$

under the constraints that the moments e and $\mathbf{f}$ be given, one obtains a Fermi–Dirac type angular dependence of the radiative distribution function

$$\mathcal{F}(\mu) = \Psi_{\rm ME}(\mu;\eta,a) = \frac{1}{e^{\eta - a\mu}+1} \quad . \tag{15}$$

Here and in the following, μ denotes the cosine of the polar angle of the momentum vector of the radiation quanta with respect to the preferential (radial) direction. Taking moments of the maximum entropy distribution $\Psi_{\rm ME}$, one obtains e, f, and p as functions of the two Lagrange multipliers η and a. The closure is formally obtained by inversion of $e(\eta,a)$ and $f(\eta,a)$ to express the Lagrange multipliers in terms of e and f. These latter relations may be used to write the closure in the form $p = p_{\rm ME}(e,f)$. MEC is thus inherently a two-dimensional closure, depending explicity on the energy density e, as well as the flux f.

In general, the functional form, Eq. (15), of the model distribution does not allow analytic inversion, $\eta(e,f)$ and $a(e,f)$. For this reason, the maximum entropy neutrino distribution was considered originally (Cernohorsky et al. 1989; Cernohorsky & van den Horn 1990) in a Pade approximation that led to the Levermore-Pomraning closure LPC (Sect. 3.2.2). However, in the case of fermionic radiation, the assumptions involved in this approximation may lead to violation of constraints imposed by the Pauli principle. Therefore, Janka et al. (1992) explored the nature of the full maximum entropy closure by performing the inversion $\eta = \eta(e,f)$ and $a = a(e,f)$ numerically. While these investigations revealed that the neutrino angular distribution is well represented by the two-parameter Fermi–Dirac form of Eq. (15), it was noted that the numerical inversion was too time consuming for MEC to be of practical use in neutrino transport calculations. However, the inversion became redundant when Cernohorsky & Bludman (1994) found a closed form for the variable Eddington factor

$$p_{\rm ME} = \frac{1}{3} + \frac{2(1-e)(1-2e)}{3}\chi\left(\frac{f}{1-e}\right) \quad . \tag{16}$$

The function χ is defined as

$$\chi(x) = 1 - 3x/q(x) \quad , \tag{17}$$

in which $q(x)$ is the inverse of the Langevin function $x \equiv L(q) \equiv \coth q - 1/q$.

The lowest-order polynomial approximation to χ, having the correct behaviour in the free-streaming and diffusive limits and no free parameters,

$$\chi(x) = x^2(3 - x + 3x^2)/5 \quad , \tag{18}$$

is accurate to at least 2%. Using this approximation in $q(x) = 3x/(1-\chi(x))$ is equivalent to interpolate between the limits $q(x) \to 3x$ for $x \to 0$, and $q(x) \to x/(1-x)$ for $x \to 1$ in the inverse Langevin function. (This has a maximum error of 8% at $x = 0.8$.) With the polynomial approximation, maximum entropy closure becomes a feasible option in two-moment transport, as the actual inversion of the Langevin function is bypassed. Fig. 1 shows $p_{\rm ME}(e,f)$ as a function of flux

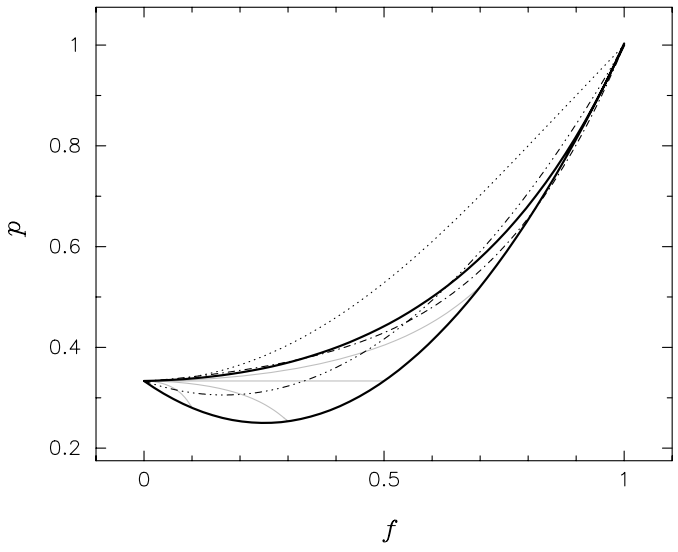

Fig. 1. Closures. Solid curves denote maximum entropy closure Eddington factors $p(e, f)$ versus flux ratio f at fixed e-values. The two fat curves mark the boundaries of maximum entropy closure. The upper fat curve is the low density limit $e = 0$, the lower one is the maximum packing curve. In between lie, with solid gray lines, from top to bottom, $e = 0.3$ to $e = 0.9$ in steps of $\Delta e = 0.2$. The dashed-dotted curve is Janka's Monte Carlo closure MCC, the dash-triple-dotted line is Wilsons minimal closure WMC, and dotted is the Levermore-Pomraning closure, LPC.

ratio f at several fixed e-values. Note that an actual solution $\{e(r),\ f(r),\ p(r)\}$ of TMT will not follow any of these curves, because $e(r)$ varies with radius.

3.1.1. Maximum packing

A limiting case of the maximum entropy distribution is obtained for

$$\lim_{\substack{a\to\infty \\ \eta/a=\mu_0}} \Psi_{\rm ME}(\mu) \equiv \Psi_{\rm MP}(\mu) = \begin{cases} 0 & (-1 < \mu < \mu_0) \\ 1 & (\mu_0 < \mu < 1) \end{cases} \quad . \tag{19}$$

Fu (1987) calls this angular degeneracy, in analogy with the zero-temperature limit of the Fermi-function in energy space: for $a \to \infty$, angular states above μ_0 are filled. Janka et al. (1992) also refer to it as "maximum (or tightest) packing": all radiation is packed in a cone with the minimal possible opening angle $\theta_0 = \arccos\mu_0$. The maximum packing distribution $\Psi_{\rm MP}$ yields, with (9) respectively, the moments $e = \frac{1}{2}(1-\mu_0)$, $f = \frac{1}{2}(1+\mu_0)$, $p = \frac{1}{3}(1+\mu_0+\mu_0^2)$. A maximum packing closure relation is readily derived:

$$p_{\rm MP}(f) = \frac{1}{3}(1 - 2f + 4f^2) \quad . \tag{20}$$

This maximum packing closure marks one boundary of maximum entropy closure in (p, f) space: in Fig. 1, $p_{\rm MP}(f)$ is the lower fat curve above which all maximum entropy trajectories $p_{\rm ME}(e, f)$ lie.

Table 1. Eddington factors for two ad hoc and three statistical one-dimensional closures. The function $q(L)$ is the inverse of the Langevin function $L(q) \equiv \coth q - 1/q$.

Closure	$p(f)$	$p'(1)$
Ad Hoc		
Wilson	$\frac{1}{3}(1 - f + 3f^2)$	5/3
Monte Carlo	$\frac{1}{3}(1 + 0.5f^{1.31} + 1.5f^{4.13})$	2.28
Statistical		
Maximum packing	$\frac{1}{3}(1 - 2f + 4f^2)$	2
Minerbo	$1 - 2f/q(f)$	2
Levermore-Pomraning	$f \coth q(f)$	1

3.1.2. Minerbo closure

The other boundary of MEC is set by the limit $\eta \gg 1 + |a|$, for which the distribution becomes $\Psi_{\rm ME}(\mu) \simeq e^{-(\eta - a\mu)}$. This is the low density or Maxwell-Boltzmann limit of MEC. The moment integrals (9) can be performed analytically and lead to Minerbo's (1978) closure

$$p_{\rm MI} = 1 - 2f/a \quad , \tag{21}$$

$$f = \coth a - 1/a \quad . \tag{22}$$

This closure is shown as the upper fat curve in Fig. 1. Together with the maximum packing curve it marks the domain of MEC in (p, f) space. The closures $p_{\rm MI}$ and $p_{\rm MP}$ both satisfy the causality requirement (13). Therefore, this approach to radial free streaming is followed by all intermediate MEC trajectories $p_{\rm ME}(e, f)$ as well. Fig. 1 also shows a number of other closures that we proceed to discuss in relation to MEC. The closures are summarized in Tables 1 and 2.

3.2. Other closures

3.2.1. Wilson's closure

Wilson's closure (WMC)

$$p_{\rm WM}(f) = \frac{1}{3} - \frac{1}{3}f + f^2 \tag{23}$$

and equivalent "minimal" flux limiter

$$\lambda(R) = \frac{1}{3 + R} \quad , \tag{24}$$

originally presented (Wilson et al. 1975) for use in flux-limited neutrino diffusion are still widely used in numerical simulations of gravitational collapse (e.g., Bowers & Wilson 1982; Wilson et al. 1975; Wilson 1984; Bruenn 1975, 1985; Mezzacappa & Bruenn 1993a, 1993b; Messer et al. 1998). Physically, the prescription amounts to an interpolation between the diffusive and free streaming fluxes by harmonically averaging the two. This guarantees the correct diffusive and free streaming limits, but leaves the intermediate behavior imprecise.

Wilson's closure, with $dp_{\rm WM}/df|_{f=1} = 5/3$, does not satisfy the causality requirement (13), and has a minimum at $f = 1/6$ (see Fig. 1). In one-dimensional closures, such a minimum is not expected as $p(f)$ is a measure of the anisotropy in

Table 2. Statistics and Angular Distribution.

Closure	Statistics	$\Psi(\mu, f)$
Maximum packing	Extreme FD	$\theta(\mu - \mu_0)\,,\ \mu_0 = 1 - 2e$
Minerbo	Maxwell-Boltzmann, $e \ll 1$	$(ea/\sinh a)\exp(a\mu)$
Levermore-Pomraning	Extreme BE, $e \gg 1$	$[\coth q(f) - f\,]\,/\,[\coth q(f) - \mu\,]$

the direction of **f**; indeed it does not occur in other conventional one-dimensional closures. In two-dimensional closures, on the other hand, $p = p(e, f)$ need not be monotonic increasing as a function of f (See also Janka et al. 1992).

3.2.2. Levermore-Pomraning closure

Another closure that has been widely adopted in both photon and neutrino radiative transfer is the Levermore-Pomraning closure (LPC), corresponding to the flux limiter of Levermore & Pomraning (1981). This closure can be parametrised by

$$p_{\rm LP} \;=\; f\,\coth R \quad , \tag{25}$$

$$f \;=\; \coth R - 1/R \quad . \tag{26}$$

The closure corresponds to an approximate angular distribution which is assumed to be slowly varying in space and time in the intermediate transport regime. (The Knudsen parameter R in this case is a slight generalization of (3).)

The closure LPC was shown to be consistent with maximum entropy considerations (Pomraning 1981). However, the closure stands out as the anomalous one in Fig. 1, where it is seen to lie outside the domain of (fermionic) MEC. The underlying distribution (see Table 2) can be derived from the maximum entropy distribution (15) by assuming $|a| \ll 1$ (Cernohorsky et al. 1989), but this assumption no longer holds away from isotropy. This by itself is not problematic, but it may cause the distribution, $\Psi_{\rm LP}(\mu)$, to exceed unity. In the case of fermions, this represents an internal inconsistency (Janka et al. 1992). To prevent it, one must impose $|a| < 1$, but a is not controllable. From a given TMT solution we may work backwards to find $\Psi_{\rm LP}(\mu; \eta, a)$ by inverting $e(\eta, a)$ and $f(\eta, a)$, and check if $\Psi_{\rm LP} < 1$ or $|a| < 1$, but *a priori* measures cannot be undertaken. Calculating the energy density with $\Psi_{\rm LP}(\mu)$ and inverting, one finds

$$a = (\coth R - e/R)^{-1} \quad , \tag{27}$$

so, at a given R, the parameter a exceeds unity when $e > e_R$, where

$$e_R = R\coth R - R \quad . \tag{28}$$

With $f(R)$ given by Eq. (26), a parametric constraint $e_R(f)$ limits e at a given f value. For a neutrino transport solution this means that $e(r)$ must drop sufficiently rapidly in the outer regions where $f(r)$ increases; else the solution is inconsistent with the fermionic nature of the radiation.

It was already pointed out by Janka (1991, 1992) and Körner & Janka (1992) that LPC pushes $f \to 1$ too rapidly in regions where the opacity drops to low values. This is related to the fact that $p_{\rm LP}(f)$ does not contain a critical point (See also Smit et al. (1997)). This behavior can be quantified by checking the approach to free streaming. For LPC one finds

$$\left(\frac{\partial p_{\rm LP}}{\partial f}\right)_{f=1} = 1 \quad , \tag{29}$$

which is a factor of two below the value required by (13), and explains why in Fig. 1, LPC lies well above the other closures.

3.2.3. Janka's Monte Carlo closure

Janka (1991, 1992) performed extensive Monte Carlo calculations of neutrino transport in typical hot neutron star environments. From the results he constructed several analytic fits $p = p_{\rm MC}(f)$ to energy averaged transport data. The fits were parametrised as

$$p_{\rm MC}(f) = \frac{1}{3}[\,1 + a\,f^m + (2-a)\,f^n\,] \quad , \tag{30}$$

and different sets (a, m, n) were provided. If we insist on the free streaming behaviour (13), the fit parameters should be related by

$$am + (2-a)n = 6 \quad . \tag{31}$$

This constraint is not satisfied by the parameters listed in Janka (1991) which show deviations up to 20%. The closure corresponding to the set ($a = 0.5$, $m = 1.3064$, $n = 4.1342$), pertains to electron-type neutrinos in a background model resembling the model M0 which we use in Sect. 4; it is denoted as MCC and is shown in Fig. 1. As noted by Janka et al. (1992), the MCC closures were in general not well represented by conventional one-dimensional closures, but could be reproduced by two-dimensional maximum entropy solutions.

4. Model calculations

4.1. Background models

Transport calculations in this paper were restricted to neutrinos of the electron type, and were performed on a stationary matter background denoted as "model M0", shown in Fig. 2. This model is a tri-polytrope representative of a hot proto-neutron star in the cooling phase following collapse and core-bounce. In Sect. 4.4 we also briefly consider "model WW1", which is an iron core halfway in collapse (central density $\rho_c = 8.8\times10^{12}$ g cm^{-3}). It has been evolved from an initial iron

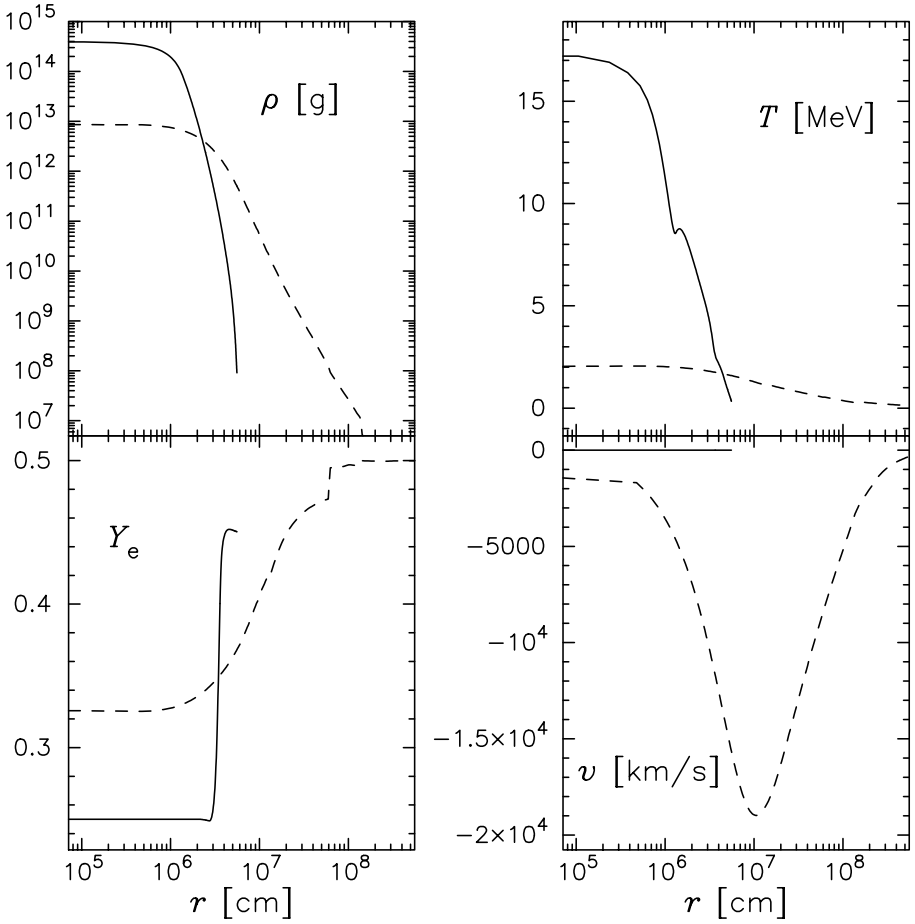

Fig. 2. Background models M0 (solid lines) and WW1 (dashed). Shown are, as a function of radius, from left to right, top down, the density ρ, temperature T, electron fraction Y_e, and infall velocity v.

core at the center of a $12\,M_\odot$ red giant of Woosley & Weaver (1995), which was kindly provided to us by S. Woosley. The evolution from the initial model with $\rho_c = 9.1 \times 10^9$ g cm^{-3} to WW1 was calculated with Newtonian hydrodynamics coupled to two-moment neutrino transport using the maximum entropy closure.

Lattimer & Swesty's (1991) equation of state was used in both models. The equation of state determines the chemical composition (mass fractions of free protons, neutrons, alpha particles and a typical nucleus) and chemical potentials, which are required to determine neutrino opacities and the equilibrium distribution. The opacities include absorption and scattering on the particles mentioned; neutrino-electron scattering and pair processes were left out (but including them would not affect the conclusions of this paper).

The next two sub-sections focus on a fixed neutrino energy, $\omega = 8.1$ MeV, roughly the average energy of the neutrinos emerging from the background model M0. In Sect. 4.4, a spectral analysis is made of the Eddington factors. From the point of view of weak and strong equivalence, we compare the TMT results with Boltzmann transport using discrete ordinate (S_N) calculations involving $N = 64$ angular bins. A mesh of 200 (unequally spaced) radial bins was used. The code is described elsewhere (Smit 1998).

4.2. Weak equivalence

We first address weak equivalence, *i.e.*, the agreement between the lowest three angular moments obtained by approximate and exact transport calculations.

Results for neutrino energy $\omega = 8.1$ MeV are shown in Fig. 3, displaying the angular moments $e(r)$, $f(r)$ and $p(r)$ versus radius. Qualitatively, all solutions exhibit the same behaviour of the 8.1 MeV radiation field. Below $r \approx 20$ km, the radiation follows equilibrium dictated by the matter, $e(r) \simeq b(r)$, while the small flux $f(r) \ll 1$ and the Eddington factor $p(r) \simeq 1/3$, indicate that the radiation is diffusive. At larger radii, $r > 20$ km, e is no longer equal to b, p differs from 1/3, and on a linear scale, f begins to deviate from zero noticeably. From an eye-on inspection of Figs. 3a-d it is hard to judge which of the TMT solutions is in better agreement with S_N, except that the LPC solution is clearly worse as the surface is approached. We will proceed with a more quantitative comparison.

Comparing the $e(r)$ profiles of TMT and S_N, good agreement is found for MEC, MCC and WMC closures which cannot be distinguished from S_N in Fig. 3a. The largest deviation of TMT-MEC is 6% (larger) at $r = 41$ km, for TMT-MCC it is 6% (smaller) at $r = 31$ km, and for TMT-WMC 9% (larger) at $r = 39$ km, all with respect to S_N. For LPC, the differences are much larger and amount to a 30% deficit at the surface.

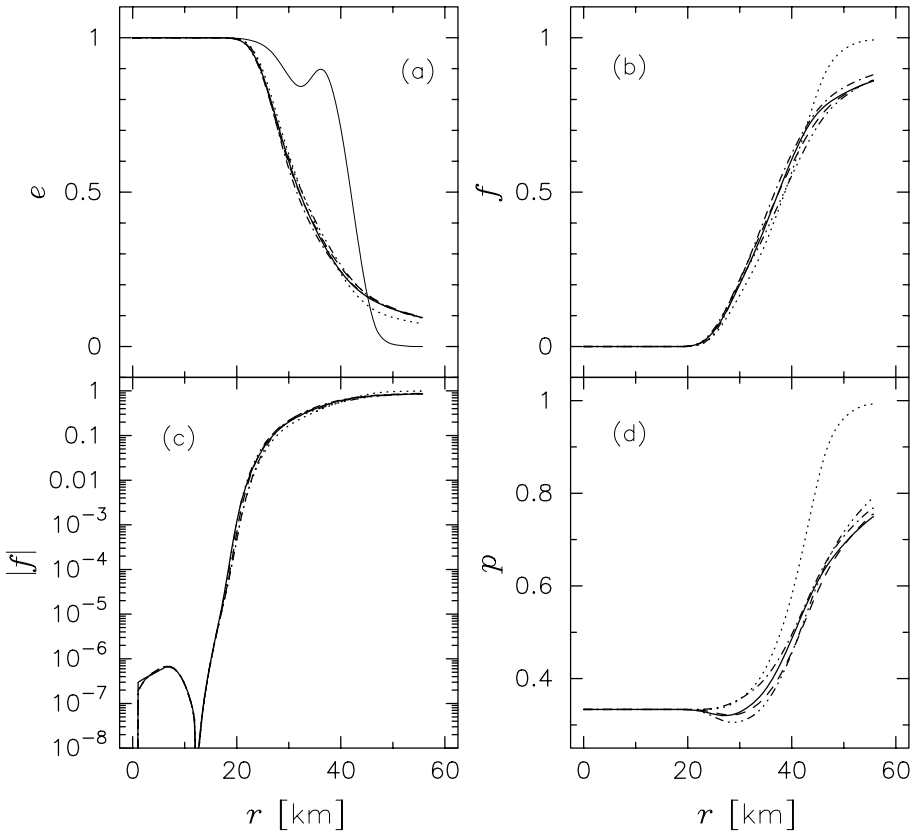

Fig. 3a–d. Stationary state neutrino transport results: angular moments $e(r)$, $f(r)$, and $p(r)$ for neutrino energy $\omega = 8.1$ MeV. Solid line is the discrete ordinate S_N solution, and dashed the two-moment transport solution with MEC closure. The other two curves are two-moment results with Janka's MCC (dash-dotted), Wilson's WMC (dash-triple-dotted), and the LPC (dotted). The flux ratio $f(r)$ is plotted twice: on a linear scale (**b**), and a logarithmic scale (**c**). To show also the negative fluxes that occur at $r < 12$ km, the absolute value is taken in **c**, causing the cusp near 12 km. Frame **a** also displays the equilibrium function $b(r)$ with a thin solid line.

Looking at $f(r)$ and $p(r)$ in Figs. 3b-d, we see the differences between the various solutions becoming apparent in the semi-transparent layer, most obviously in the case of the LPC solution. LPC reaches parallel free streaming, $f \to 1$ and $p \to 1$ at the surface, where the other solutions have f and p still well below these limiting values. The tendency of LPC to push towards a purely radial flow ($f, p \to 1$) too rapidly was already referred to in Sect. 3.2.2. An additional point to note is that the TMT-LPC solution obtained here does not satisfy the fermion-constraint discussed in that section *anywhere* in the iron core, *i.e.*, the occupation density $e(r)$ exceeds the limiting value given by Eq. (28) at all radii.

For $f(r)$ and $p(r)$, there is again fair agreement between S_N and TMT for all closures except LPC, although larger differences are observed than in the case of $e(r)$. Nevertheless, these differences are too small to stand out clearly in the plots. The flux ratio $f_{\rm ME}(r)$ computed with MEC, is found to approximate $f_{S_N}(r)$ to better than 9% at radii larger than 25 km. Below this radius, the overall differences are in the range 10-20%, but they cannot be discerned in the figure. Near the surface, $f_{\rm ME}$ and f_{S_N} practically coincide. The MCC and WMC flux ratios, $f_{\rm MC}$ and $f_{\rm WM}$, agree with MEC for $r < 17$ km, but in the semi-transparent region and out to the surface, they differ from MEC and from each other. The magnitude by which they differ from f_{S_N} is in the same range as was found for $f_{\rm ME}$.

Fig. 3d shows that just beyond $r = 20$ km the Eddington factors $p(r)$ begin to visibly deviate from $1/3$, and, for different solutions, also deviate from each other. A special feature to note is that $p_{S_N}(r)$, $p_{\rm ME}(r)$ and $p_{\rm WM}(r)$ drop below $1/3$ at radii $20 < r < 31$ km. This is impossible for the one-dimensional closures MCC and LPC. The MEC and WMC solutions mimic S_N with a precision better than 2% and 5%, respectively. However, for WMC, $p(f) < 1/3$ is imposed by construction, whereas MEC contains it as a possible solution trajectory.

Finally, in Fig. 3d, in the approach to free streaming, all two-moment Eddington factors except LPC are close to the S_N solution, with MEC providing a slightly better fit. At the surface, MEC, MCC, WMC, and LPC deviate by 1, 2, 4 and 43%, respectively.

Based on this monochromatic calculation, we have no clear-cut indication to favour a particular closure, although the numbers are slightly better for TMT-MEC. On the other hand, TMT-LPC is clearly disfavoured, as was already anticipated in Sect. 3.2.2.

4.3. Strong equivalence

We now turn to strong equivalence, a good correspondence between the actual angular distribution $\mathcal{F}(r, \mu)$ and a certain model distribution $\Psi(r, \mu)$. While both closures MEC and LPC were derived from model distributions, LPC already fails to give weak equivalence. For strong equivalence we will therefore consider only MEC. In Sect. 3.1 we noted that the maximum entropy model distribution is a two-parameter function, containing the two Lagrange multipliers η and a used in the maximalization procedure, see Eq. (15). This function, $\Psi_{\rm ME}(r, \mu; \eta, a)$, can be

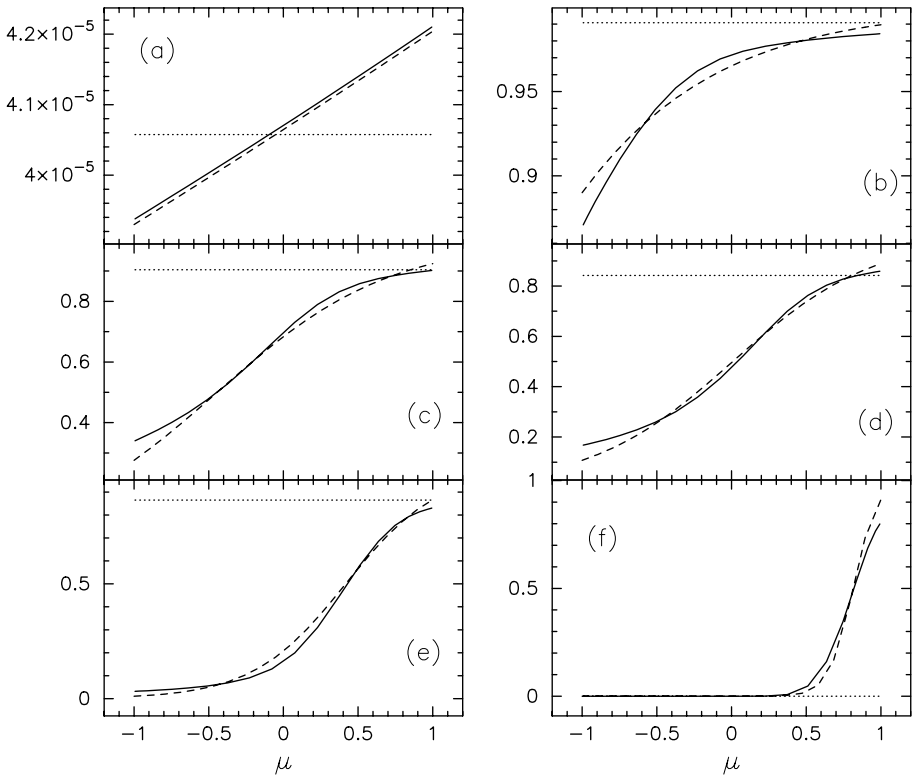

Fig. 4a–f. Angular dependence of the $\omega = 8.1$ MeV distribution function at six different positions in model M0. Solid line is $\mathcal{F}(r,\mu)$ from S_N transport, the dashed line is the distribution $\Psi_{\rm ME}(r,\mu;\eta,a)$ associated with MEC two-moment transport. The equilibrium function b is indicated with a dotted line. The successive plots are at radial positions r =8.6, 23, 29, 32, 38, 55 km, with corresponding neutrino depth $\tau = 2.6\times10^{2}$, 2.9×10^{0}, 6.4×10^{-1}, 2.9×10^{-1}, 6.4×10^{-2}, 9.6×10^{-6}. Frame (**a**) shows $[1-\mathcal{F}(\mu)]$ and $[1-\Psi_{\rm ME}(\mu)]$ (and $[1-b]$).

calculated *a posteriori* from a TMT-MEC calculation of $e_{\rm ME}(r)$, $f_{\rm ME}(r)$ by (numerical) inversion of the set of equations

$$e_{\rm ME}(r) \;=\; \frac{1}{2}\int_{-1}^{1} d\mu\,\Psi_{\rm ME}(r,\mu;\eta,a) \qquad (32)$$

$$f_{\rm ME}(r) \;=\; \frac{1}{2e_{\rm ME}}\int_{-1}^{1} d\mu\mu\,\Psi_{\rm ME}(r,\mu;\eta,a) \quad , \qquad (33)$$

to obtain $\eta(e(r),f(r))$ and $a(e(r),f(r))$ at a particular radius. Fig. 4 shows the discrete ordinate distribution $\mathcal{F}(r,\mu)$ and the model distribution $\Psi_{\rm ME}(r,\mu;\eta,a)$ as functions of polar angle at six radial positions of decreasing neutrino depth in model M0, at neutrino energy $\omega = 8.1$ MeV. Table 3 lists the values of a and η at these positions, and the angular moments e, f from both solutions.

Fig. 4a does not display $\mathcal{F}$ and $\Psi_{\rm ME}$, but rather their deviations from unity, $[1-\mathcal{F}]$ and $[1-\Psi_{\rm ME}]$. The figure shows that at this large neutrino depth radiation is very nearly isotropic: both $\mathcal{F}$ and $\Psi_{\rm ME}$ deviate from unity by a minute fraction. Note that the figure displays textbook diffusion: the distribution function is linear in the cosine of the polar angle, the Eddington factor $p = 1/3$, and the diffusion approximation holds to a high degree of accuracy. The diffusive flux has negative sign here (cf. Fig. 3c).

The other frames, (b)-(f), show how, moving out towards the stellar surface, radiation becomes forward peaked. Deviation from near isotropy is seen in frame (b) at neutrino depth $\tau = 3$, as well as non-linearity in the angular dependence, signaling the breakdown of the diffusion approximation. In Table 3, a increases with decreasing depth, and η changes from a large negative to a large positive value. The MEC distribution $\Psi_{\rm ME}$ is point-symmetric around $\mu = \mu_0 = \eta/a$ (maximum packing), with angular states above $\mu = \mu_0$ more populated than below. In frames (c)-(e), μ_0 is in the range $-1 < \mu_0 < 1$, and can be associated with a real angle $\theta_0 = \arccos\mu_0$. The angle θ_0 decreases outwards, in agreement with peaking of the radiation getting stronger.

The profiles in frames (c)-(e) suggest Pauli-blocking in angle space (a left-right mirrored Fermi-function) (cf. Janka 1991, Janka et al. 1992). The blocking level is, however, below one. Only if the blocking level reaches one can we be sure that angular Pauli-blocking is observed. From the set of graphs in Janka (1991, his Fig. 3.12) the blocking level cannot be inferred because the data are averaged over neutrino energy and normalised with respect to the local neutrino density. We may conclude from Figs. 4a-f that, on the whole, $\Psi_{\rm ME}(\mu)$ matches $\mathcal{F}(\mu)$ remarkably well considering that it is only a two-parameter function: it is able to reproduce the overall character of the radiation field, which changes from a simple linear dependence on polar angle to being highly forward peaked.

4.4. Spectral Eddington factors

Earlier sections focused on a monochromatic solution of the neutrino Boltzmann and two-moment equations. As remarked, a comparison of the two should involve the energy dependence of the radiation field, and TMT should provide an adequate approximation to the Boltzmann solution at more than one neutrino energy. It is not intended here to repeat the monochromatic analysis of the previous sections at multiple energies. However, based on a comparison of the angular moments, our calculations

Table 3. For six positions in the star shown in Fig. 4, this table lists e and f as obtained with the S_N method (second and third column) and the TMT method (fourth and fifth). The last three columns list the Lagrange multipliers a and η corresponding to a given TMT-MEC set (e, f), and the angle $\mu_0 = \eta/a$.

	$S_{N=20}$		TMT-MEC				
#	e	f	e	f	a	η	μ_0
(a)	1-4.07 10^{-5}	-4.56 10^{-7}	1-4.07 10^{-5}	-4.57 10^{-7}	-3.37 10^{-2}	-1.01 10^{+1}	3.0 10^{2}
(b)	9.57 10^{-1}	1.70 10^{-2}	9.57 10^{-1}	1.62 10^{-2}	1.23 10^{0}	-3.32 10^{0}	-2.7 10^{0}
(c)	6.65 10^{-1}	1.64 10^{-1}	6.51 10^{-1}	1.81 10^{-1}	1.80 10^{0}	-7.81 10^{-1}	-4.3 10^{-1}
(d)	5.03 10^{-1}	2.77 10^{-1}	4.97 10^{-1}	2.98 10^{-1}	2.16 10^{0}	1.74 10^{-2}	8.1 10^{-3}
(e)	3.03 10^{-1}	5.08 10^{-1}	3.12 10^{-1}	5.13 10^{-1}	3.29 10^{0}	1.36 10^{0}	4.1 10^{-1}
(f)	9.75 10^{-2}	8.36 10^{-1}	9.72 10^{-2}	8.59 10^{-1}	1.25 10^{+1}	1.02 10^{+1}	8.2 10^{-1}

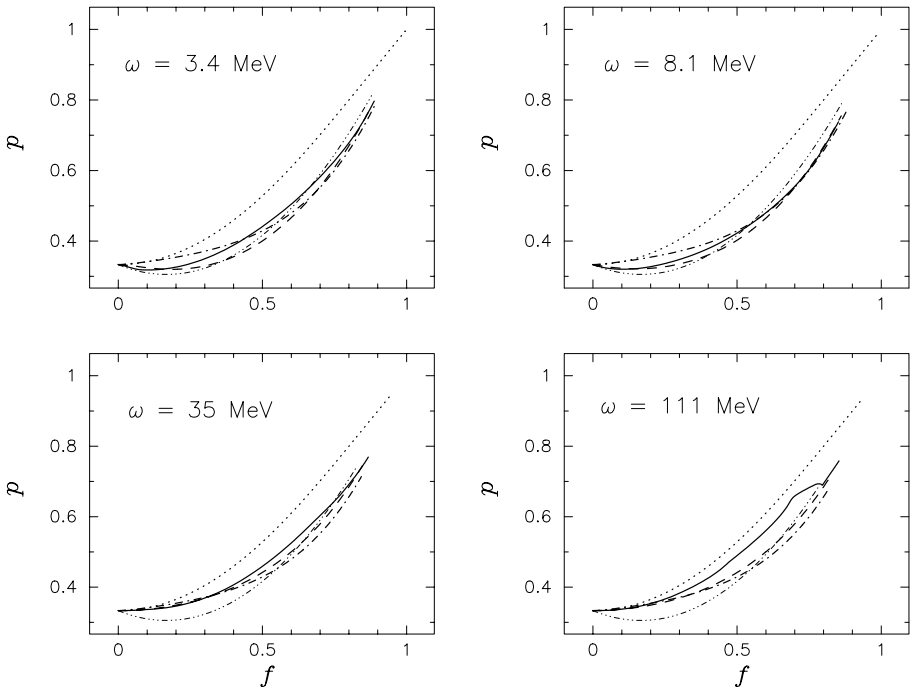

Fig. 5. Eddington factors $p(f)$ versus flux ratio f of S_N and TMT neutrino transport on model M0, at four different energies (values are indicated in the figures). Solid lines correspond with S_N, dashed with two-moment MEC, dash-dotted with MCC, dash-triple dotted with WMC, and dotted with LPC.

for several energies do support weak equivalence of the MEC solutions.

An alternative multiple-energy test of TMT versus S_N can be made by looking at the variable Eddington factor as a function of f, like a one dimensional closure. The nature of the radiation field is for a large part contained in how $p(f)$ behaves as a function of f alone. This is clear, because if the relationship $p(f)$ were known for the true radiation field, it could be used in the two-moment equations to find the exact solutions $e(r)$ and $f(r)$. In Fig. 5, $p(f)$ trajectories are plotted for four neutrino energies. While the one-dimensional closures MCC, WMC en LPC remain the same in all four plots, it is clear that the Eddington trajectory $p_{S_N}(f)$ is different at each neutrino energy. The Eddington trajectories of TMT-MEC, $p_{\rm ME}(f)$, are also different, and, due to the additional freedom of MEC in (f, p) space, are able to follow $p_{S_N}(f)$ more closely on average. Notice in particular that TMT-MEC, in accordance with S_N, has a minimum in the Eddington trajectories of the lower two energies, while at the higher two energies, TMT-MEC does not display this minimum, again in agreement with S_N.

For $f > 0.5$, all closures except LPC have Eddington trajectories that agree with S_N equally well. But at the highest energy, $\omega = 111$ MeV, it is actually LPC that gives the best overall fit. At this energy, the $p_{\rm ME}(f)$ curve in Fig. 5 coincides with the top fat curve in Fig. 1, *i.e.*, the Minerbo closure $p_{\rm MI}(f)$. Because the density of these high energy neutrinos is very low in the atmosphere, MEC tunes to the Minerbo closure which is the low density limit $e \to 0$. For $\omega = 111$ MeV, the curve $p_{S_N}(f)$ lies outside the dynamic range of MEC in (f-p) space, *i.e.*, in the semi-transparent regime the radiation field is peaked more strongly than MEC can account for. Cernohorsky & Bludman (1994) claim that fermionic radiation should be confined

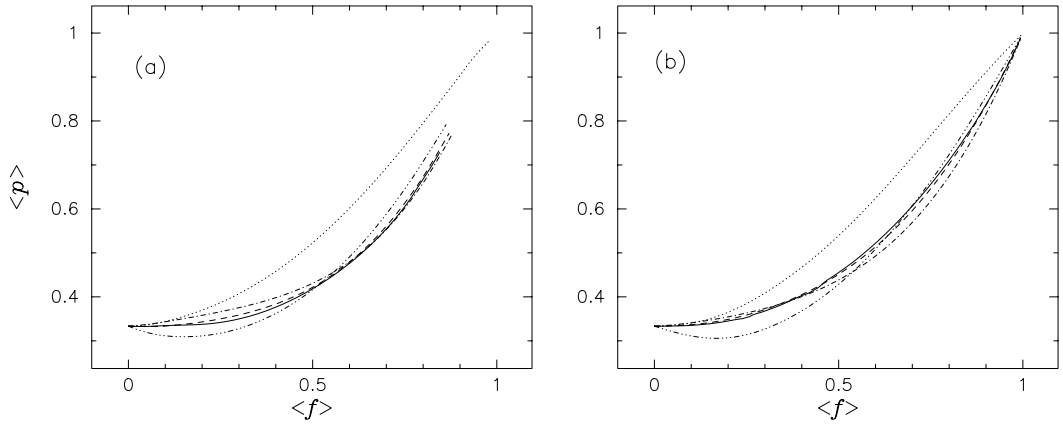

Fig. 6a,b. Energy averaged Eddington factors $\langle p\rangle$ versus average flux ratio $\langle f\rangle$ in model M0 **a** and model WW1 **b**. Solid lines correspond with S_N, dashed with two-moment MEC, dash-dotted with MCC, dash-triple-dotted with WMC, and dotted with LPC.

to the fermionic MEC (f-p) domain. Here we see that this need not be so: there is no reason why a *particular* neutrino radiation field need comply with a *statistical* maximum entropy principle. In fact, $p_{S_N}(f)$ lies within the bosonic maximum entropy domain which is bounded by the Minerbo curve and the Levermore-Pomraning curve.

High energy neutrinos in the semi-transparent regions have relatively small weight due to their low abundance. Deviations of TMT with respect to S_N at these energies may, therefore, not be so important. We check on this by considering the energy-averaged moments,

$$\langle f\rangle(r) = \frac{\int d\omega\omega^3 e(r,\omega) f(r,\omega)}{\int d\omega\omega^3 e(r,\omega)} \quad , \tag{34}$$

and

$$\langle p\rangle(r) = \frac{\int d\omega\omega^3 e(r,\omega) p(r,\omega)}{\int d\omega\omega^3 e(r,\omega)} \quad . \tag{35}$$

The average Eddington factor $\langle p\rangle$ versus $\langle f\rangle$ is shown in Fig. 6a for S_N and TMT with different closures. For this exercise, all transport calculations were performed with 25 energy groups in the range $[0, 250]$ MeV. Agreement between TMT-MEC and S_N is excellent: at a given average flux $\langle f\rangle$, average TMT-MEC and S_N Eddington factors differ from each other by 3% at most. The energy averaged TMT-MCC Eddington trajectory, within 6% of S_N, is just about as good,

For TMT to be useful, weak equivalence must always apply. Background model M0 is only one snapshot in the sequel of core collapse events. Therefore, we consider another matter background, model WW1, already described in Sect. 4.1. Its temperature, density and other parameters are shown (dashed) in Fig. 2. An additional reason to consider this model is that the atmosphere of model M0 does not extend to very large radii (an artifact of the polytropic model). As a result, we could not explore the entire (f-p) space: calculations reached to $f = 0.9$, $p = 0.8$, leaving a gap towards $f = p = 1$, the radial streaming limit.

We compare, as before, energy averaged Eddington factors from S_N and TMT calculations. Because model WW1 is less dense and cooler than model M0, the neutrino energy range was lowered to 85 MeV (still using 25 bins). Average Eddington factors are shown in Fig. 6b; again we find good agreement between S_N and TMT-MEC, with differences between the two of 2% only, while TMT-MCC agrees to within 6%. The aforementioned atmospheric gap is bridged along the nearly linear track $\partial_f p|_{f=1} = 2$ (with the expected exception of LPC).

5. Conclusions

We have computed numerical neutrino transport using two methods: a discrete ordinate method, S_N, to obtain a direct solution of the Boltzmann equation, and two-moment transport, TMT, with a variable Eddington factor. The two were compared first by looking at the angular moments $\{e,\ f,\ p\}$, *i.e.,* weak equivalence of the radiation field $\mathcal{F}$. Four different closures, MEC, WMC, LPC, and MCC were used in TMT. Of these, LPC is not weakly equivalent to the three moments in S_N. The remaining three closures, MEC, MCC, and WMC, give more or less the same, good accuracy in monochromatic transport, with maximum entropy closure (MEC) being slightly the better of the three. In addition to weak equivalence, MEC displayed strong equivalence at this typical energy, *i.e.,* the maximum entropy distribution function, $\Psi_{\rm ME}(r,\mu)$, as a function of polar angle, gave a fair enough description of the radiation field $\mathcal{F}(r,\mu)$ as calculated with the S_N method.

Spectral solutions of S_N showed that the Eddington trajectories $p(f)$ are different at different energies. One-dimensional closures are unable to account for this, but $p_{\rm ME}(e,f)$, the two-dimensional closure MEC, has extra freedom in (f-p) space. Thus, for example, MEC can follow a $p < 1/3$ trajectory. The closure of Wilson, WMC, does have a minimum where $p < 1/3$, but will always invoke it in a TMT solution, even when the actual radiation field may not display this feature. The MEC trajectories may cover a domain bounded by the limiting curves representing the Minerbo and maximum packing closure relations. In their approach to free streaming, all of these trajectories obey the causality constraint (13) (as do the S_N solutions). While MCC can be constructed to also meet this requirement,

the closures WMC and LPC always violate this condition. In the low density regime the S_N solution may be closely tracked by the Minerbo limit of MEC. On the other hand, the maximum packing limit was never attained in the S_N solutions. Therefore, in our experience, Minerbo's closure may lead to a good representation of non-diffusive neutrino transport, but maximum packing cannot be recommended as a closure. The closure LPC, although originally shown to be consistent with maximum entropy considerations, lies essentially outside the domain of fermionic MEC.

Very good agreement between TMT-MEC and S_N was found in the energy averaged Eddington trajectories $\langle p \rangle$ versus $\langle f \rangle$, indicating that the neutrino spectrum is on average well represented by TMT-MEC. This was also found for TMT-MCC, but with TMT-MEC again being superior. This average weak equivalence of TMT-MEC/MCC and S_N was found for two different background models, representing an early and a late stage of core collapse. We may, therefore, expect that TMT-MEC and TMT-MCC are likely to give an accurate average representation of the neutrino radiation field during the entire core collapse scenario.

In this respect let us mention that velocity dependent terms encountered in actual dynamical (or relativistic) calculations introduce the third order moment (beyond f and p), for which a convenient practical inversion scheme is lacking. While from a given angular model distribution one can calculate the moments, in the case of the maximum entropy angular distribution a practical closure on the third order moment would be available only in the Minerbo and maximum packing limits. Another example is the third moment of the LP-distribution (see Van Thor et al. 1995), which of course will fail the weak equivalence requirement. The Minerbo and maximum packing closures, on the other hand, may be as adequate as discussed.

Summarizing, two-moment transport (TMT) gave the best overall fit to the discrete ordinate (S_N) solution when using the maximum entropy (MEC) and Janka's Monte Carlo (MCC) closures. In view of its physical basis and greater p-f domain, we favour MEC over MCC as a closure in two-moment neutrino transport.

Acknowledgements. S.A.B. is supported in part by U.S. Department of Energy grant DE-FG02-95ER40893.

References

Anile A.M., Pennisi S., Sammartino M., 1991, J. Math. Phys. 32, 544
Bruenn S.W., 1975, Ann. N.Y. Acad. Sci. 262, 80
Bruenn S.W., 1985, ApJS 58, 771
Bowers R.L., Wilson J.R., 1982, ApJ 263, 366
Cernohorsky J., Bludman S.A., 1994, ApJ 433, 205
Cernohorsky J., van den Horn L.J., 1990, J. Quant. Spectr. Rad. Transfer 43, 33
Cernohorsky J., van den Horn L.J., Cooperstein J., 1989, J. Quant. Spectr. Rad. Transfer 42, 603
Dgani R., Janka H.-Th., 1992, A&A 256, 428
Fu A., 1987, ApJ 323, 227
Janka H.-Th., 1991, Ph.D. Thesis, Techn. Univ. München
Janka H.-Th., 1992, A&A 256, 452
Janka H.-Th., Dgani R., van den Horn L.J., 1992, A&A 265, 345
Körner A., Janka H.-Th., 1992, A&A 266, 613
Lattimer J.M, Swesty F.D., 1991, Nuc. Phys. A 535, 331
Levermore C.D., 1984, J. Quant. Spectr. Rad. Transfer 31, 149
Levermore C.D., Pomraning G.C., 1981, ApJ 248, 321
Messer O.E.B., Mezzacappa A., Bruenn S.W., Guidry M.W., 1998, ApJ 507, 353
Mezzacappa A., Bruenn S.W., 1993a, ApJ 405, 637
Mezzacappa A., Bruenn S.W., 1993b, ApJ 410, 740
Minerbo G.N., 1978, J. Quant. Spectr. Rad. Transfer 20, 541
Pomraning G.C., 1981, J. Quant. Spectr. Rad. Transfer 26, 385
Smit J.M., 1998, Ph.D. Thesis, Univ. of Amsterdam
Smit J.M., Cernohorsky J., Dullemond C., 1997, A&A 325, 203
Van Thor W.F., Dgani R., van den Horn L.J., Janka H.-Th., 1995, A&A 298, 863
Wilson J.R., 1984, In: Centrella J., LeBlanc J., Bowers R.L. (eds.) Numerical Astrophysics. Joan & Bartlett Publ., Inc., Boston
Wilson J.R., Couch R., Cochran S., LeBlanc J., 1975, Ann. N.Y. Acad. Sci. 262, 54
Woosley S.E., Weaver T.A., 1995, ApJS 101, 181